JOC Article
pubs.acs.org/joc

Computational Investigation of the Reaction Mechanisms of Nitroxyl and Thiols

Matthew P. Sherman, Whitney R. Grither, and Ryan D. McCulla*

Department of Chemistry, Saint Louis University, 3501 Laclede Avenue, Saint Louis, Missouri 63103

rmccull2@slu.edu

Received February 1, 2010

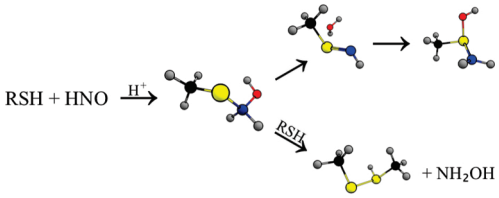

Nitroxyl, or nitrosyl hydride, (HNO) is a pharmacologically relevant molecule whose physiological responses have been thought to result from modification of intracellular thiols. The reaction of HNO with thiols has been shown to lead to disulfides and sulfinamides. The free energies of reaction (ΔG) and activation ($\Delta G^{\ddagger}$) were determined for the reaction pathways of HNO and five different thiols using computational methods. The methods employed included B3LYP, MP2, and CBS-QB3, as well as IEF-PCM to approximate implicit water solvation. The five examined thiols were hydrogen sulfide, methanethiol, trifluoromethanethiol, thiophenol, and cysteine. A putative *N*-hydroxysulfenamide intermediate was the initial product for the reaction of HNO with a thiol. Analysis of the Wiberg bond indices indicated that the formation of the S−N bond was concerted with the proton transfers that led to the intermediate. The calculated pK_a of protonated *N*-hydroxysulfenamide was approximately 13, and from the protonated *N*-hydroxysulfenamide intermediate, two irreversible reactions that lead to either the disulfide or sulfinamide were found. The calculated values of $\Delta G^{\ddagger}$ indicated the preferred reaction pathway would be dependent upon the hydrophobicity of the environment, the availability of a local base, and the identity of the thiol substituent. In a hydrophobic environment, the formation of the disulfide was kinetically favored. Formation of the sulfinamide product was expected to occur upon the protonation of the hydroxy group of the *N*-hydroxysulfenamide intermediate.

I. Introduction

Nitroxyl or nitrosyl hydride (HNO), a redox congener of nitric oxide, has been shown to possess many unique and beneficial pharmacological properties.[1,2] A number of studies have shown the potential for therapeutic applications of HNO in a variety of diseases, which include treatments for heart failure and alcohol abuse.[3−7] For example, the adverse physiological response to alcohol ingestion brought on by cyanamide treatments has been postulated to result from the release of HNO after oxidation of cyanamide by catalase.[8] Additionally, HNO donors afforded neuroprotection from excitotoxic assault by downregulating *N*-methyl-D-aspartate (NMDA) receptors.[9] Nitroxyl has been shown to be a

(1) Paolocci, N.; Jackson, M.; Lopez, B.; Miranda, K.; Tocchetti, C.; Wink, D.; Hobbs, A.; Fukuto, J. *Pharmacol. Ther.* **2007**, *113* (2), 442–458.
(2) Fukuto, J. M.; Bartberger, M. D.; Dutton, A. S.; Paolocci, N.; Wink, D. A.; Houk, K. N. *Chem. Res. Toxicol.* **2005**, *18* (5), 790–801.
(3) Paolocci, N.; Katori, T.; Champion, H.; St John, M.; Miranda, K.; Fukuto, J.; Wink, D.; Kass, D. *Proc. Natl. Acad. Sci. U.S.A.* **2003**, *100* (9), 5537–5542.
(4) Tocchetti, C. G.; Wang, W.; Froehlich, J. P.; Huke, S.; Aon, M. A.; Wilson, G. M.; Di Benedetto, G.; O'Rourke, B.; Gao, W. D.; Wink, D. A.; Toscano, J. P.; Zaccolo, M.; Bers, D. M.; Valdivia, H. H.; Cheng, H.; Kass, D. A.; Paolocci, N. *Circ. Res.* **2007**, *100* (1), 96–104.
(5) Pagliaro, P.; Mancardi, D.; Rastaldo, R.; Penna, C.; Gattullo, D.; Miranda, K. M.; Feelisch, M.; Wink, D. A.; Kass, D. A.; Paolocci, N. *Free Radicals Biol. Med.* **2003**, *34* (1), 33–43.
(6) Feelisch, M. *Proc. Natl. Acad. Sci. U.S.A.* **2003**, *100* (9), 4978–80.
(7) DeMaster, E. G.; Redfern, B.; Nagasawa, H. T. *Biochem. Pharmacol.* **1998**, *55* (12), 2007–15.
(8) Nagasawa, H. T.; DeMaster, E. G.; Redfern, B.; Shirota, F. N.; Goon, D. J. *J. Med. Chem.* **1990**, *33* (12), 3120–2.
(9) Kim, W.; Choi, Y.; Rayudu, P.; Das, P.; Asaad, W.; Arnelle, D.; Stamler, J.; Lipton, S. *Neuron* **1999**, *24* (2), 461–469.

Published on Web 05/19/2010 DOI: 10.1021/jo100172t

thiophilic electrophile, and many of the HNO-mediated physiological responses have been postulated to result from the modification of intracellular thiols.[7−10]

Rate constants for the reaction of HNO and several thiols have been experimentally measured. The rate constant for the reaction of glutathione (GSH) with HNO was reported as $2 \times 10^6\ M^{-1}\ s^{-1}$; however, the rate constant for *N*-acetylcysteine (NAC), which has been used as a HNO scavenger, was appreciably slower at $5 \times 10^5\ M^{-1}\ s^{-1}$.[10] The reactivity of protein thiols toward HNO was dependent upon the active site environment. For example, the rate constant for bovine serum albumin (BSA) was near $6 \times 10^6\ M^{-1}\ s^{-1}$, whereas the rate constant for glyceraldehyde-3-phosphate dehydrogenase (GAPDH) was estimated to be greater than $1 \times 10^9\ M^{-1}\ s^{-1}$.[11] The enhanced reactivity of GAPDH was attributed to general base catalysis through deprotonation of the critical cysteine by a histidine residue.[12] Thus, the pK_a of the thiol and the hydrophobicity of the local environment have been postulated to affect the reactivity of thiols toward HNO.

A number of studies have shown that incubation of enzymes with critical cysteine residues in the presence of HNO donors results in reversible or irreversible inhibition of enzymatic activity.[5,11−24] Modification of important cysteine residues was suspected of being the cause of the observed HNO-mediated inhibition. In an early attempt to identify possible reaction products, the reaction of HNO with thiophenol was reported to generate phenyl disulfide and hydroxylamine (NH_2OH).[25] As shown in Scheme 1, the initial reaction between HNO and a thiol (**1**) was speculated to generate a *N*-hydroxysulfenamide (**2**) intermediate that could undergo a facile reaction with an additional thiol moiety to yield the disulfide (**3**) and NH_2OH. Disulfides are susceptible to exchange with free thiols or reduction by systems such as glutaredoxin in vivo, both of which would be expected to result in the regeneration of the active form of the enzyme.[20,26] Therefore, the reaction pathway leading to disulfides has been used to explain reversible inhibition of GAPDH by HNO under certain conditions.[13,21]

The formation of a sulfinamide (**4**) from the reaction of HNO and a thiol was proposed as the irreversible modification responsible for prolonged inhibition of protein function.[7,12,21−24] Support for this assignment came from an unknown product with a mass spectrum consistent with cyclohexanesulfinamide being observed after the reaction of HNO with cyclohexyl mercaptan.[27] Loss of hydroxide from **2** was proposed to give rise to alkyliminosulfonium (**5**), whose subsequent reaction with water would be expected to produce the observed sulfinamide product. More recent mass spectrometry studies revealed that in the absence of free cysteine, human calbindin (HCalB) and GAPDH, both of which contain critical cysteines, gave rise to ions consistent with the conversion of thiols into sulfinamides after incubation with the known HNO donor Angeli's salt ($Na_2N_2O_3$).[28] Formation of the sulfinamide adduct could be prevented with the addition of free thiols before, but not after, exposure to HNO.[28]

Nitroxyl was found to inhibit glycolysis in whole yeast cells by presumably forming an irreversible adduct with GAPDH.[12] Surprisingly, the observed inhibition occurred without altering the redox status of intracellular GSH, which indicated the selectivity of a thiol for HNO was dependent upon the local environment. Interestingly, the inhibition of GADPH in vitro was prevented by the addition of a low concentration of GSH.[21] A possible explanation for the in vitro protection against HNO-mediated inhibition of GAPDH by the addition of low concentrations of GSH was rapid scavenging of HNO by GSH. An alternative explanation was that **2** was rapidly converted to the reversible disulfide modification by GSH before the biologically irreversible rearrangement to **5** could occur. It was postulated that GAPDH possesses favorable characteristic for facile reactions with HNO, which would favor the latter mechanistic explanation. However, GSH protection of GAPDH in vitro but not for whole cell preparations likely results from the difference between the in vitro and whole cell environments, and thus, neither mechanistic explanation completely explains the apparent contradiction.

Despite the importance of biological thiols to the potential pharmacology of HNO, little is known about the specific factors that dictate the formation of the disulfide or sulfinamide products. Experimentally determining these factors is complicated by nitroxyl's spontaneous dimerization to form hyponitrous acid, as well as the *N*-hydroxysulfenamide intermediates and sulfinamide products often being unstable and difficult to isolate.[29,30] In this work, computational methods are used to investigate the reaction pathways of HNO with thiols and to examine which aspects influence the bifurcated reaction pathways of putative intermediate **2**.

(10) Miranda, K. M.; Paolocci, N.; Katori, T.; Thomas, D. D.; Ford, E.; Bartberger, M. D.; Espey, M. G.; Kass, D. A.; Feelisch, M.; Fukuto, J. M.; Wink, D. A. *Proc. Natl. Acad. Sci. U.S.A.* **2003**, *100* (16), 9196–201.
(11) Flores-Santana, W.; Switzer, C.; Ridnour, L. A.; Basudhar, D.; Mancardi, D.; Donzelli, S.; Thomas, D. D.; Miranda, K. M.; Fukuto, J. M.; Wink, D. A. *Arch. Pharm. Res.* **2009**, *32* (8), 1139–53.
(12) Lopez, B. E.; Rodriguez, C. E.; Pribadi, M.; Cook, N. M.; Shinyashiki, M.; Fukuto, J. M. *Arch. Biochem. Biophys.* **2005**, *442* (1), 140–148.
(13) Tao, L.; English, A. M. *Biochemistry* **2004**, *43* (13), 4028–38.
(14) Shirota, F. N.; DeMaster, E. G.; Shoeman, D. W.; Nagasawa, H. T. *Toxical. Lett.* **2002**, *132* (1), 1–8.
(15) Cook, N. M.; Shinyashiki, M.; Jackson, M. I.; Leal, F. A.; Fukuto, J. M. *Arch. Biochem. Biophys.* **2003**, *410* (1), 89–95.
(16) Arnelle, D. R.; Stamler, J. S. *Arch. Biochem. Biophys.* **1995**, *318* (2), 279–85.
(17) Lee, M.; Nagasawa, H.; Elberling, J.; DeMaster, E. *J. Med. Chem.* **1992**, *35* (20), 3648–3652.
(18) Miller, T. W.; Cherney, M. M.; Lee, A. J.; Francoleon, N. E.; Farmer, P. J.; King, S. B.; Hobbs, A. J.; Miranda, K. M.; Burstyn, J. N.; Fukuto, J. M. *J. Biol. Chem.* **2009**, *284* (33), 21788–96.
(19) Zeller, A.; Wenzl, M. V.; Beretta, M.; Stessel, H.; Russwurm, M.; Koesling, D.; Schmidt, K.; Mayer, B. *Mol. Pharmacol.* **2009**, *76* (5), 1115–22.
(20) Starke, D. W.; Chock, P. B.; Mieyal, J. J. *J. Biol. Chem.* **2003**, *278* (17), 14607–13.
(21) Lopez, B.; Wink, D.; Fukuto, J. *Arch. Biochem. Biophys.* **2007**, *465* (2), 430–436.
(22) Vaananen, A. J.; Salmenpera, P.; Hukkanen, M.; Miranda, K. M.; Harjula, A.; Rauhala, P.; Kankuri, E. *Free Radic. Biol. Med.* **2008**, *45* (6), 749–755.
(23) Vaananen, A.; Salmenpera, P.; Hukkanen, M.; Rauhala, P.; Kankuri, E. *Free Radical Biol. Med.* **2006**, *41* (1), 120–131.
(24) Väänänen, A. J.; Kankuri, E.; Rauhala, P. *Free Radical Biol. Med.* **2005**, *38* (8), 1102–11.
(25) Doyle, M.; Mahapatro, S.; Broene, R.; Guy, J. *J. Am. Chem. Soc.* **1988**, *110* (2), 593–599.
(26) Bach, R. D.; Dmitrenko, O.; Thorpe, C. *J. Org. Chem.* **2008**, *73* (1), 12–21.
(27) Wong, P. S. Y.; Hyun, J.; Fukuto, J. M.; Shirota, F. N.; DeMaster, E. G.; Shoeman, D. W.; Nagasawa, H. T. *Biochemistry* **1998**, *37* (16), 5362–5371.
(28) Shen, B.; English, A. M. *Biochemistry* **2005**, *44* (42), 14030–14044.
(29) Shafirovich, V.; Lymar, S. V. *Proc. Natl. Acad. Sci. U.S.A.* **2002**, *99* (11), 7340–7345.
(30) Kohout, F.; Lampe, F. *J. Am. Chem. Soc.* **1965**, *87* (24), 5795–5796.

SCHEME 1

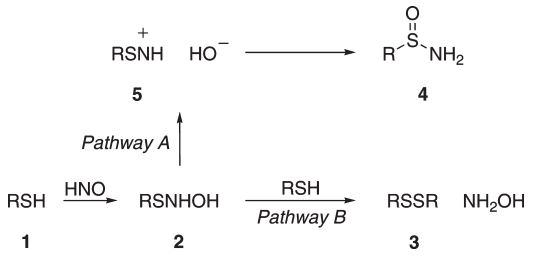

II. Computational Methods

To find the lowest energy conformations of the reactants and products, rationally selected conformers were optimized at the HF/6-31G(d) level of theory. Initial guess transitions states were also found at this level of theory. From the set of HF/6-31G(d)-optimized conformational geometries, only the lowest energy conformer was further refined at the B3LYP/6-31G(d) and PCM-B3LYP/6-31G(d) levels of theory. Polarizable continuum model (PCM), specifically the integral equation formalism (IEF-PCM), was also used to model the reactions in water.[31] Graphical renderings and tables of critical bond lengths of all of the computed structures are given in the Supporting Information, and in general, only the structures critical to the discussion are included in this manuscript.

The B3LYP/6-31G(d)-optimized structures were used for B3LYP/6-311+G(d), B3LYP/6-311+G(3d,2p), B3LYP/6-311+G(3df,2p), MP2/6-311G(3d,2p), MP2/6-311+G(3d,2p), and MP2/6-311+G(3df,2p) single-point energies. Additionally, the CBS-QB3 level of theory was used to explore the gas-phase potential energy surface.[32] The energies of the PCM-B3LYP/6-31G(d)-optimized structures were further refined using PCM-B3LYP/6-311+G(d), PCM-B3LYP/6-311+G(3d,2p), PCM-B3LYP/6-311+G(3df,2p), PCM-MP2/6-311G(3d,2p), PCM-MP2/6-311+G(3d,2p), and PCM-MP2/6-311+G(3df,2p) levels of theory.

Hessians were obtained to classify the nature of every stationary point, to obtain the harmonic vibrational frequencies, and to provide zero-point energy corrections, which were all scaled in accordance with the work by Scott and Radom.[33] The reported ΔG and $\Delta G^{\ddagger}$ were calculated from the absolute energies, the scaled ZPE, and the thermal and entropic contributors to free energy at 298.15 K, which all were obtained from the B3LYP/6-31G(d) or PCM-B3LYP/6-31G(d) vibrational frequency calculations using unmodified frequencies. Intrinsic reaction coordinate (IRC) calculations were used to confirm that all transition states connect the reactants and products.[34] All calculations were performed with the Gaussian 03 suite of programs, and natural bond orbital calculations were run using NBO version 3.1.[35,36] Results were visualized with the ChemCraft software program.[37]

SCHEME 2

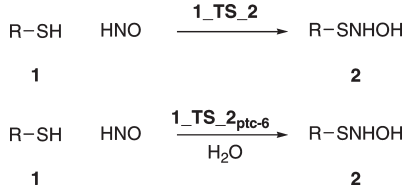

Using previously reported procedures, pK_a values were estimated from the reaction free energy for the neutralization of a given acid by water.[38−41] A thermodynamic cycle involving the gas phase reaction free energy and the solvation energies of the associated species was used to determine the reaction free energy in solution. Solvation free energies were determined using IEF-PCM calculations on the PCM-B3LYP/6-31G(d) geometries at several different levels of theory. Gas-phase free energies were determined as described above.

Previous work suggested that 6-311+G(2df,p) or larger basis sets were required to obtain reliable structures for nitrosothiol complexes.[42] For the first reaction shown in Scheme 2, the critical structures for R = CH_3 were additionally optimized at the B3LYP/6-311+G(2df,p) level of theory. The S−N bond length of **2** (R = CH_3) was 1.70 and 1.73 Å for the B3LYP/6-31G(d) and B3LYP/6-311+G(2df,p) geometries, respectively. Energy refinements of the B3LYP/6-31G(d)- and B3LYP/6-311+G(2df,p)-optimized structures at the MP2/6-311+G(3df,2p) level of theory were used to determine ΔG for the reaction. The level of theory used to generate the equilibrium geometries had little effect on the calculated values of ΔG (−9.0 and −9.5 kcal/mol). Given the size of the larger thiols, it was concluded that the B3LYP/6-31G(d)- and PCM-B3LYP/6-31G(d)-optimized structures were an acceptable compromise of efficiency and accuracy sufficient for reasonable estimates of ΔG and $\Delta G^{\ddagger}$.

III. Results and Discussion

IIIA. Reaction of HNO and Thiols. The expected product of the reaction of HNO and a thiol (**1**) was the putative *N*-hydroxysulfenamide intermediate (**2**), as shown in Scheme 2. The formation of the S−N bond and the transfer of the S−H proton of **1** to the oxygen of HNO were the key processes in this reaction. In solution, solvent molecules potentially assist the proton transfer from sulfur to oxygen. Therefore, a transition-state structure, where an explicit solvent water molecule (**1_TS_2$_{ptc-6}$**) acted as a proton-transport catalyst, was considered. The notation X_TS_Y_{ptc-z} will be used throughout this manuscript to describe transition state structures that connect a starting reactant (X) and product (Y). A subscripted "ptc" will be used to indicate the involvement of explicit water as a proton-transport catalyst that facilitates the formation a Z-membered cyclic transition

(31) Tomasi, J.; Mennucci, B.; Cammi, R. *Chem. Rev.* **2005**, *105* (8), 2999–3093.
(32) Montgomery, J. A.; Frisch, M. J.; Ochterski, J. W.; Petersson, G. A. *J. Chem. Phys.* **1999**, *110* (6), 2822–2827.
(33) Scott, A. P.; Radom, L. *J. Phys. Chem.* **1996**, *100* (41), 16502–16513.
(34) Fukui, K. *Acc. Chem. Res.* **1981**, *14* (12), 363–368.
(35) Frisch, M. J.; Trucks, G. W.; Schlegel, H. B.; Scuseria, G. E.; Robb, M. A.; Cheeseman, J. R.; Montgomery, J. A., Jr.; Vreven, T.; Kudin, K. N.; Burant, J. C.; Millam, J. M.; Iyengar, S. S.; Tomasi, J.; Barone, V.; Mennucci, B.; Cossi, M.; Scalmani, G.; Rega, N.; Petersson, G. A.; Nakatsuji, H.; Hada, M.; Ehara, M.; Toyota, K.; Fukuda, R.; Hasegawa, J.; Ishida, M.; Nakajima, T.; Honda, Y.; Kitao, O.; Nakai, H.; Klene, M.; Li, X.; Knox, J. E.; Hratchian, H. P.; Cross, J. B.; Bakken, V.; Adamo, C.; Jaramillo, J.; Gomperts, R.; Stratmann, R. E.; Yazyev, O.; Austin, A. J.; Cammi, R.; Pomelli, C.; Ochterski, J. W.; Ayala, P. Y.; Morokuma, K.; Voth, G. A.; Salvador, P.; Dannenberg, J. J.; Zakrzewski, V. G.; Dapprich, S.; Daniels, A. D.; Strain, M. C.; Farkas, O.; Malick, D. K.; Rabuck, A. D.; Raghavachari, K.; Foresman, J. B.; Ortiz, J. V.; Cui, Q.; Baboul, A. G.; Clifford, S.; Cioslowski, J.; Stefanov, B. B.; Liu, G.; Liashenko, A.; Piskorz, P.; Komaromi, I.; Martin, R. L.; Fox, D. J.; Keith, T.; Al-Laham, M. A.; Peng, C. Y.; Nanayakkara, A.; Challacombe, M.; Gill, P. M. W.; Johnson, B.; Chen, W.; Wong, M. W.; Gonzalez, C.; Pople, J. A. *Gaussian 03*; Gaussian, Inc.: Wallingford, CT, 2003.
(36) *Gaussian NBO*, 3.1.
(37) Zhurko, G. A.; Zhurko, D. A. *ChemCraft 1.5*; **2007**.
(38) Namazian, M.; Halvani, S. *J. Chem. Thermodyn.* **2006**, *38* (12), 1495–1502.
(39) da Silva, E.; Svendsen, H. *Ind .Eng. Chem. Res.* **2003**, *42*, 4414–4421.
(40) Pliego, J. R.; Riveros, J. M. *J. Phys. Chem. A* **2002**, *106* (32), 7434–7439.
(41) Chipman, D. M. *J. Phys. Chem. A* **2002**, *106* (32), 7413–7422.
(42) Baciu, C.; Gauld, J. *J. Phys. Chem. A* **2003**, *107* (46), 9946–9952.

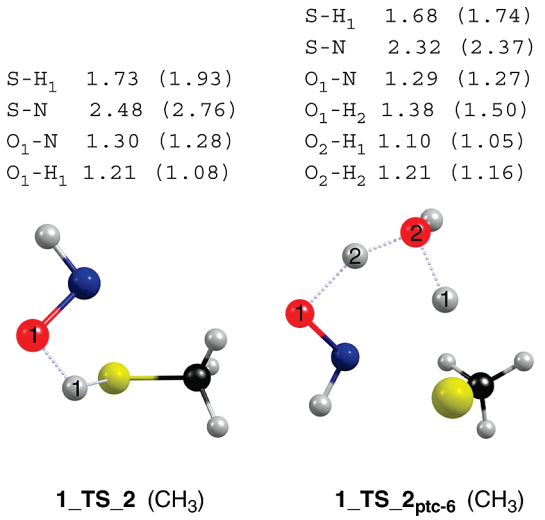

FIGURE 1. Graphical renderings of the B3LYP/6-31G(d) structures of **1_TS_2** and **1_TS_2**$_{ptc-6}$ displaying the B3LYP/6-31G(d) and (PCM-B3LYP/6-31G(d)) bond distances (Å): carbon (black), hydrogen (gray), nitrogen (blue), oxygen (red), sulfur (yellow).

state. Additionally, the notation X·Y will be used to indicate an intermolecular complex between X and Y. To investigate potential substituent effects, the reactions of HNO and five different thiols, hydrogen sulfide (R = H), methanethiol (R = CH_3), trifluoromethanethiol (R = CF_3), thiophenol (R = Ph), and the amino acid cysteine (R = Cys), were examined.

For the reaction between HNO and **1**, the bond lengths for bonds that undergo a significant change in bond order are reported in Table S1, Supporting Information. The identity of the substituent had little effect on the critical geometric parameters for the reactants, transitions states, and products. The transition state structure (**1_TS_2**) connected the product **2** to a dipole−dipole complex (**1·HNO**) of **1** and HNO, which was a minimum on the potential energy surface. Likewise, **1_TS_2**$_{ptc-6}$ was found to connect intermolecular bound complexes corresponding to the reactant and products. However, for both transition states, the complexes were endergonic compared to the completely isolated reactant and products at the CBS-QB3 level of theory, and therefore, they were not examined further.

The examined substituents had little effect on the geometries of **1_TS_2** and **1_TS_2**$_{ptc-6}$, and thus, methanethiol (**1**, R = CH_3), whose transition states structures **1_TS_2** and **1_TS_2**$_{ptc-6}$ are shown in Figure 1, can be used as an illustrative example. For simplicity, the values given in this manuscript are for R = CH_3 unless stated otherwise. In the transition states (**1_TS_2** and **1_TS_2**$_{ptc-6}$), the S−H_1 bond of **1** (1.35 Å) had already significantly lengthened to 1.73 and 1.68 Å for **1_TS_2** and **1_TS_2**$_{ptc-6}$, respectively. Consequent with the lengthened S−H_1 distance was a short O−H_1 distance for the proton-accepting oxygen (O_1 for **1_TS_2** and O_2 for **1_TS_2**$_{ptc-6}$). Intrinsic reaction coordinate (IRC) calculations, for both **1_TS_2** and **1_TS_2**$_{ptc-6}$, showed that transfer of the S−H proton to the oxygen of HNO accompanied S−N bond formation. For **1_TS_2**$_{ptc-6}$, transfer of the proton to the oxygen of HNO lagged behind the removal of the S−H_1 proton by the explicit solvent water.

The relative progress of the bond-breaking and -forming processes at **1_TS_2** and **1_TS_2**$_{ptc-6}$ were estimated from the relative change of Wiberg bond indices (∂B_i) as defined by eq 1. For eq 1, the superscripts R, TS, and P represent the reactant, transition state, and product, respectively. In the gas phase, the percent changes in the bond indices for S−H, S−N, O−N, and O−H bond of **1_TS_2** were 54.9%, 55.9%, 55.2%, and 50.0%, respectively. For **1_TS_2**$_{ptc-6}$, the S−H, S−N, O_1−N, and O_2−H_1 percent change in the bond indices were all approximately 50%; however, the proton transfer from the explicit water to HNO (O_1−H_2, and O_2−H_2) had only progressed 35% toward completion, which reflects the analysis of the bond lengths. Moyano and co-workers defined the absolute asynchronicity (A) of a chemical reaction using eq 2, where $\partial B_{i(avg)}$ was the average change of the bond indices and n was the number of bonds undergoing change.[43] Larger A values correspond to a more asynchronous reaction.[43] The A values for the reaction of CH_3SH with HNO were 0.02 and 0.08 for **1_TS_2** and **1_TS_2**$_{ptc-6}$, respectively, which indicated that S−N bond formation and the proton transfers were essentially synchronous.

$$\delta B_i = [B_i^{TS} - B_i^{R}]/[B_i^{P} - B_i^{R}] \quad (1)$$

$$A = (1/2n-2)\sum(|\partial B_i - \partial B_{i(avg)}|/\partial B_{i(avg)}) \quad (2)$$

The ΔG and $\Delta G^{\ddagger}$ for the reaction of HNO and thiols were determined at several levels of theory. For the gas phase, the CBS-QB3 energies were considered the most accurate since CBS-QB3 used rigorous methods that were extrapolated to a complete basis set.[32] In other studies, CBS-QB3 energies have been combined with PCM-B3LYP/6-311+G(d) estimations of ΔG of aqueous solvation to approximate a PCM-CBS-QB3 value.[44] However, a fully integrated PCM-CBS-QB3 method has not been developed, and thus, PCM models were only used in conjunction with MP2 and B3LYP methods. While several basis sets were used, methods using larger basis sets were considered the most reliable due to the requirement that tight d orbitals be included for accurate energies of sulfur containing molecules.[45] Additionally, barrier heights are systematically underestimated at the B3LYP level, and therefore, the PCM-MP2/6-311+G(3df,2p)//PCM-B3LYP/6-31G(d) was considered the best level of theory for accurate estimates of ΔG and $\Delta G^{\ddagger}$ in aqueous solutions.[46] With these considerations, only the CBS-QB3

TABLE 1. Free Energies of Reaction and Activation for the Reaction between Thiols (1) and HNO To Form *N*-Hydroxysulfenamides (2)[a]

R	level of theory	$\Delta G^{\ddagger}_{1\_TS\_2}$	$\Delta G^{\ddagger}_{1\_TS\_2ptc-6}$	$\Delta G_{1\rightarrow 2}$
H	CBS-QB3	50.5	40.4	−2.2
	PCM-MP2/6-311+G(3df,2p)[b]	63.4	48.1	−7.7
CH_3	CBS-QB3	49.6	37.8	−7.9
	PCM-MP2/6-311+G(3df,2p)[b]	64.3	46.8	−10.2
CF_3	CBS-QB3	51.2	35.4	−2.7
	PCM-MP2/6-311+G(3df,2p)[b]	56.4	43.1	−7.0
Ph	CBS-QB3	--[c]	36.6	−7.2
	PCM-MP2/6-311+G(3df,2p)[b]	65.3	48.0	−9.0
Cys	CBS-QB3	48.1	38.9	−8.3
	PCM-MP2/6-311+G(3df,2p)[b]	70.6	56.0	−7.4

[a]All Gibbs free energies in kcal/mol at 298.15 K. [b]Single points at PCM-B3LYP/6-31G(d) geometries. [c]Value unavailable. Convergence of SCF failed despite multiple attempts.

(43) Moyano, A.; Pericas, M. A.; Valenti, E. *J. Org. Chem.* **1989**, *54*, 573–582.
(44) Dutton, A. S.; Fukuto, J. M.; Houk, K. N. *Inorg. Chem.* **2005**, *44* (11), 4024–8.
(45) McCulla, R. D.; Jenks, W. S. *J. Org. Chem.* **2003**, *68* (20), 7871–9.
(46) Zhao, Y.; Truhlar, D. G. *Acc. Chem. Res.* **2008**, *41* (2), 157–67.

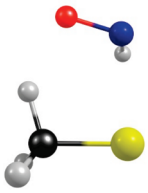

6

FIGURE 2. Sulfur−nitrogen distances for structure **6** at several levels of theory with a 6-31G(d) basis set: MP2/6-31G(d) structure depicted (R = CH_3).

and PCM-MP2/6-311+G(3df,2p)//PCM-B3LYP/6-31G(d) values are reported in Table 1 and all subsequent tables. Corresponding tables complete with all of the employed methods can be found in the Supporting Information.

Consistent with previous results, the overall reaction for all thiols with HNO was exergonic.[47,48] The inclusion of an explicit water in the transition states resulted in lower activation barriers by ~15 kcal/mol, which indicated that removal of the S−H proton facilitates the reaction. Therefore, the pK_a of **1** would be expected to influence reactivity toward HNO. This finding was consistent with the previous assertion that proteins containing critical thiols that were susceptible to general base catalysis by neighboring residues would also be sensitized toward HNO inhibition.[12,22] The magnitudes of the calculated activation energies were significantly out of line with experimentally determined rate constants, which indicated the barriers were less than 10 kcal/mol.[10,11] An explanation for this discrepancy could be the result of the experimental rate constants being measured at physiological pH where deprotonation of a portion of the reacting thiols would be expected. The nucleophilicity of a thiol increases substantially upon conversion to the corresponding thiolate.[49]

The initial reaction of a thiolate and HNO would be expected to yield the conjugate base of **2**. Unexpectedly, attempts to locate an equilibrium geometry at the HF, B3LYP, MP2, and PCM-B3LYP level of theory with the standard 6-31G(d) basis set resulted in an ion−dipole complex (**6**), shown in Figure 2, and not the conjugate base of **2**. In Figure 2, the MP2/6-31G(d) geometry of **6**, which had the shortest S−N bond length, is shown. The Wiberg bond index for the S−N bond was 0.45 at the MP2/6-31G(d) geometry, and a concomitant decrease in the bond indices was observed with the lengthening of the S−N distance for the other examined methods. Therefore, the reactivity of HNO and thiolates could not be determined using these computational methods. Without this information a definitive characterization of the reaction of HNO and thiols was not possible; however, the calculated values of $\Delta G^{\ddagger}$ for **1** and HNO suggest that deprotonation of the thiol during or prior to the rate-determining step may be a requirement.

IIIB. Reactions Leading from *N*-Hydroxysulfenamides (2) to Sulfinamides (4). As stated previously, *N*-hydroxysulfenamides have been postulated to form sulfinamides (pathway A) through a multistep rearrangement involving an alkyliminosulfonium (**5**) intermediate. In the gas phase, the loss of hydroxide from **2** leading directly to **5** can be intuitively rejected since HO^- is a poor leaving group. Indeed, the lowest calculated ΔG for the loss of HO^- from any of the examined *N*-hydroxysulfenamides (**2**) was for *N*-hydroxyphenylsulfenamide (R = Ph), which was 167.2 kcal/mol endergonic at the CBS-QB3 level of theory. At PCM-MP2/6-311+G(3df,2p), the ΔG was substantially less endergonic due to the implicit solvation of the charged products. However, the average value of ΔG was 33.8 kcal/mol for the five substituents examined and was not considered further due to the pK_a values of protonated **2**, which will now be discussed.

TABLE 2. Calculated pK_a Values of Protonated *N*-Hydroxysulfenamides[a]

R	method[b]	pK_a
H	PCM-MP2/6-311+G(3df,2p)	13.4
CH_3	PCM-MP2/6-311+G(3df,2p)	11.7
CF_3	PCM-MP2/6-311+G(3df,2p)	5.7
Ph	PCM-MP2/6-311+G(3df,2p)	13.0
Cys	PCM-MP2/6-311+G(3df,2p)	15.3

[a]All pK_a values were calculated with H_2O as solvent at 298.15 K. [b]PCM-B3LYP/6-31G(d) geometries.

Protonation of the nitrogen atom of **2** (**2H**$^+$) resulted in pK_a values ranging from 5.7 to 15.3 at the PCM-MP2/6-311+G(3df,2p)//PCM-B3LYP/6-31G(d) level of theory as shown in Table 2. Excluding the outlying *N*-hydroxytrifluoromethylsulfenamide (R = CF_3) value, the pK_a values for **2H**$^+$ ranged from 11.7 to 15.3. Thus, protonation of **2** at physiological conditions would be expected. As expected, inductive withdrawal by the trifluoromethyl group significantly lowers the pK_a.

Interestingly, no equilibrium geometries could be located when the −OH group of **2** was protonated (RSNHOH$_2^+$). A dissociative curve leading to water and an alkyliminosulfonium (**5**) was revealed by performing relaxed scans from 0.8 to 3.5 Å along the N−O bond. Since RSNHOH$_2^+$ was not a stable structure, a true pK_a for the −OH$_2^+$ protons of RSNHOH$_2^+$ could not be determined. However, if constrained to the N−O bond lengths associated with **2**, the "quasi-pK_a" values for RSNHOH$_2^+$ were all below −1.0. Comparison of the pK_a of **2H**$^+$ and the quasi-pK_a of RSNHOH$_2^+$ suggested protonation of the nitrogen atom would be strongly favored in solution.

Given the pK_a of **2H**$^+$, the rearrangement of **2** into **4** will likely involve **2H**$^+$ as an intermediate. The observed dissociation of **2** upon protonation of the −OH group indicates that a proton transfer from the nitrogen to the oxygen of **2H**$^+$ will result in the formation of **5**. In the absence of any intermolecular assistance, the 1,2-hydrogen shift proceeds through a transition state (**2H**$^+$**_TS_5·W**) that leads to an ion−dipole complex (**5·W**) between **5** and water (**W**, instead of H_2O, is used to simplify the X_TS_Y notation). Graphical renderings of the B3LYP/6-31G(d) structures for R = CH_3 are embedded in the reaction coordinate diagram shown in Figure 3. As would be expected for the transfer of a proton to a more electronegative atom, the unassisted 1,2-hydrogen shifts have considerable activation barriers of over 30 kcal/mol. Inclusion of implicit solvation raises the barriers by 6−17 kcal/mol as shown in Table 3.

A salient change during the 1,2-hydrogen shift was the decrease in the S−N bond distance from 1.81 Å for **2H**$^+$ (R = CH_3) to 1.64 Å for transition-state structure **2H**$^+$**_TS_5·W**, which represented 66% progress toward the value of 1.54 Å in

(47) Jackson, M. I.; Han, T. H.; Serbulea, L.; Dutton, A.; Ford, E.; Miranda, K. M.; Houk, K. N.; Wink, D. A.; Fukuto, J. M. *Free Radic. Biol. Med.* **2009**, *47* (8), 1130–9.
(48) Bartberger, M. D.; Fukuto, J. M.; Houk, K. N. *Proc. Natl. Acad. Sci. U.S.A.* **2001**, *98* (5), 2194–2198.
(49) Lienhard, G.; Jencks, W. *J. Am. Chem. Soc.* **1966**, *88* (17), 3982–3995.

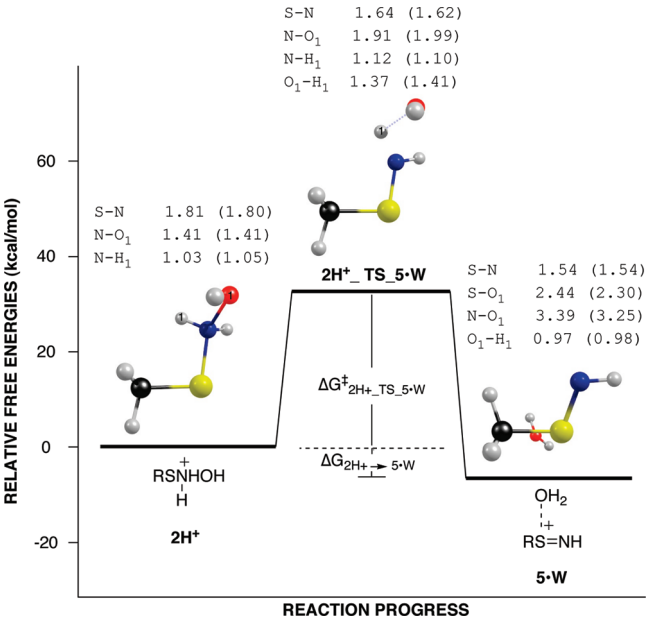

FIGURE 3. Reaction coordinate diagram for the conversion of $2H^+$ to $5\cdot W$ at the CBS-QB3 level of theory for R = CH_3. Graphical renderings of the B3LYP/6-31G(d) structures of $2H^+$, $2H^+$_TS_$5\cdot W$, and $5\cdot W$ listing the B3LYP/6-31G(d) and (PCM-B3LYP/6-31G(d)) bond distances (Å).

TABLE 3. Activation and Reaction Free Energies for Unassisted 1,2-Hydrogen Shift of $2H^+$ Leading to $5\cdot W$[a]

R	level of theory	$\Delta G^{\ddagger}_{2H^+\_TS\_5\cdot W}$	$\Delta G_{2H^+\rightarrow 5\cdot W}$
H	CBS-QB3	36.9	−4.7
	PCM-MP2/6-311+G(3df,2p)[b]	51.5	10.3
CH_3	CBS-QB3	32.5	−22.1
	PCM-MP2/6-311+G(3df,2p)[b]	38.6	−15.9
CF_3	CBS-QB3	35.6	−13.5
	PCM-MP2/6-311+G(3df,2p)[b]	52.5	0.1
Ph	CBS-QB3	30.7	−25.9
	PCM-MP2/6-311+G(3df,2p)[b]	41.9	−14.1
Cys	CBS-QB3	36.2	−20.5
	PCM-MP2/6-311+G(3df,2p)[b]	49.5	−16.8

[a]All Gibbs free energies in kcal/mol at 298.15 K. [b]Single points at PCM-B3LYP/6-31G(d) geometries.

TABLE 4. Progress of the Wiberg Bond Indices (∂B_i) for the Transition States Associated with the Conversion of $2H^+$ to 5[a]

	$2H^+$_TS_$5\cdot W$	$2H^+\cdot$W_TS_$5_{ptc\text{-}3}$	$2H^+\cdot$W_TS_$5_{ptc\text{-}5}$
S−N	42.5[b]	13.3	15.1
$N-O_1$	46.9	7.7	11.1
$N-H_1$	33.0	88.4	83.9
O_1-H_1	26.4	8.6	
O_1-H_2			19.9
O_2-H_1		65.3	74.7
O_2-H_2			26.0

[a]All values determined from NBO analysis at the B3LYP/6-31G(d) level of theory. [b]Values are percentages of the progress of the change of the bond indices for the examined transition states.

$5\cdot W$. Also, the N−O bond on average had increased 0.5 Å. This was in direct contrast to the N−H and O−H bond distances. The N−H bond on average had only increased 0.1 Å, and the O−H bond was on average still 0.4 Å away from its length for $5\cdot W$. The notion of a lagging proton transfer was supported by evaluation of the progress of the Wiberg bond indices at $2H^+$_TS_$5\cdot W$, which are given in Table 4. The progress of the bond indices indicated that S−N double bond formation and

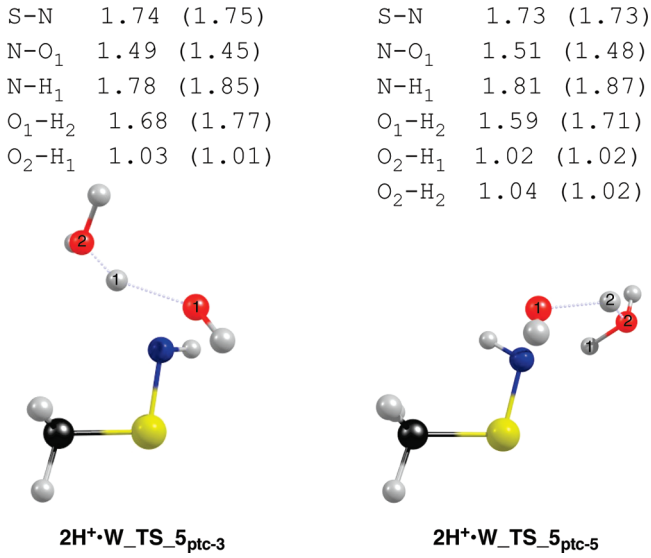

FIGURE 4. Graphical renderings of the B3LYP/6-31G(d) structures of $2H^+\cdot$W_TS_$5_{ptc\text{-}3}$ and $2H^+\cdot$W_TS_$5_{ptc\text{-}5}$ displaying the B3LYP/6-31G(d) and (PCM-B3LYP/6-31G(d)) bond distances (Å) for R = CH_3.

N−O bond breaking were ~45% complete, whereas the proton transfer was only ~30% completed at $2H^+$_TS_$5\cdot W$.

In solution, solvent water molecules may assist the 1,2-hydrogen shift by acting as proton-transport catalysts. Several possible proton-transport catalysis mechanisms were considered by including an explicit water molecule in the transition state. First, the effect of hydrogen bonding between the explicit water and one of the "non-transferring" protons of $2H^+$ throughout the reaction was considered. Initial investigations revealed that hydrogen bonding between the explicit water and either of the "non-transferring" N−H or −OH protons resulted in $\Delta G^{\ddagger}$ that were comparable to the unassisted barriers. Therefore, these mechanisms were not pursued further, and the focus was shifted to active participation of the explicit water in the proton transfer.

Two mechanisms by which the explicit water actively catalyzed the 1,2-hydrogen shift were considered. Through hydrogen bonding to the transferring N−H proton, the explicit water could assist the proton transfer by "dragging" the N−H proton to the −OH group ($2H^+\cdot$W_TS_$5_{ptc\text{-}3}$). Second, the explicit water could remove the N−H proton while simultaneously donating one of its own to the −OH group creating a 5-membered cyclic transition state ($2H^+\cdot$W_TS_$5_{ptc\text{-}5}$). These two transition state structures are shown in Figure 4. In the reverse direction, IRC calculations led to a hydrogen-bonded complex between $2H^+$ and the explicit water ($2H^+\cdot W$) for both transition states. In the forward direction, transfer of a proton to the oxygen of $2H^+\cdot W$ led to a substantial lengthening of the N−O distance; however, despite multiple attempts, an equilibrium geometry for the intermolecular complex of **5** and two water molecules could not be found along the IRC pathway. Given the dissociation of **2** upon protonation of the oxygen, the significant lengthening of the N−O bond was considered sufficient to conclude that $2H^+\cdot$W_TS_$5_{ptc\text{-}3}$ and $2H^+\cdot$W_TS_$5_{ptc\text{-}5}$ connect $2H^+$ with **5**.

Animation of the one imaginary frequency of $2H^+\cdot$W_TS_$5_{ptc\text{-}3}$ revealed a pendulum motion for H_1. Analysis of the bond lengths revealed that only the N−H and O_2-H_1 bond distances had drastically changed from $2H^+$ to

TABLE 5. Activation and Reaction Energies with Explicit Water Proton-Transport Catalysts for the 1,2-Hydrogen Shift of $2H^+$ Leading to 5.[a]

R	level of theory	$\Delta G_{2H^+ \rightarrow 2H^+ \cdot W}$	$\Delta G^{\ddagger}_{2H^+ \cdot W\_TS\_5ptc\text{-}3}$	$\Delta G^{\ddagger}_{2H^+ \cdot W\_TS\_5ptc\text{-}5}$	$\Delta G_{2H^+ \rightarrow 5+H2O}$
H					
	CBS-QB3	−11.8	21.3	18.9	−3.1
	PCM-MP2/6-311+G(3df,2p)[b]		22.2	23.2	−7.0
CH_3					
	CBS-QB3	−9.9	24.6	21.2	−14.5
	PCM-MP2/6-311+G(3df,2p)[b]		19.8	22.4	−18.0
CF_3					
	CBS-QB3	−13.8	16.4	15.3	−4.8
	PCM-MP2/6-311+G(3df,2p)[b]		11.8	15.1	−6.0
Ph					
	CBS-QB3	−8.0	21.1	21.2	−21.1
	PCM-MP2/6-311+G(3df,2p)[b]		24.9	22.8	−21.5
Cys					
	CBS-QB3	−5.2	27.5	24.4	−18.5
	PCM-MP2/6-311+G(3df,2p)[b]		23.0	24.0	−25.8

[a]All Gibbs free energies at 298.15 K. [b]Single points at PCM-B3LYP/6-31G(d) geometries.

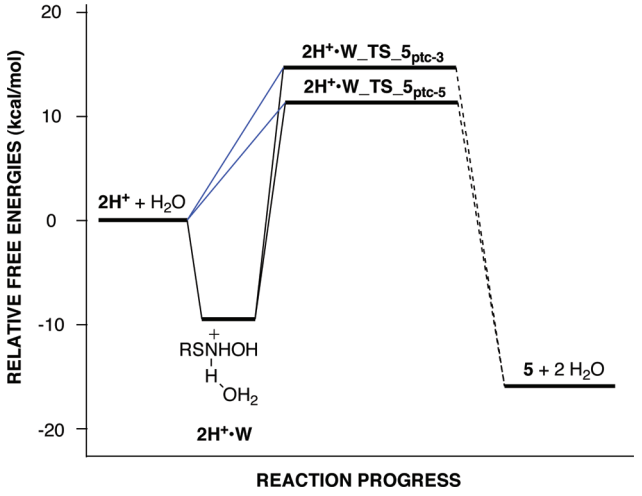

FIGURE 5. Reaction coordinate diagram for the proton-transport-catalyzed conversion of $\mathbf{2H^+}$ to **5** R = CH_3 using CBS-QB3 (black line) and PCM-MP2/6-311+G(3df,2p) (blue line) at 298.15 K.

$\mathbf{2H^+ \cdot W\_TS\_5_{ptc\text{-}3}}$. The N−$H_1$ distance had lengthened from 1.03 Å for $\mathbf{2H^+}$ to 1.78 Å in the transition state. The 1.03 Å for the O_2−H_1 bond length of $\mathbf{2H^+ \cdot W\_TS\_5_{ptc\text{-}3}}$ was comparable with the 0.99 Å O−H bond length of H_3O^+. As shown in Table 4, analysis of the progress of the Wiberg bond indices at $\mathbf{2H^+ \cdot W\_TS\_5_{ptc\text{-}3}}$ showed that transfer of the proton to the explicit water (N−H_1 and O_2−H_1) was greater than 65% completed, while the other bonds associated with $\mathbf{2H^+}$ remained less than 15% changed. Thus, for $\mathbf{2H^+ \cdot W\_TS\_5_{ptc\text{-}3}}$, the explicit solvent water assisted the 1,2-proton transfer by acting as a general base that removes the proton from the nitrogen and transports it to the −OH group.

For $\mathbf{2H^+ \cdot W\_TS\_5_{ptc\text{-}5}}$, the explicit water assisted proton transfer by removing the N−H_1 proton while transferring one of its own protons (H_2) to the oxygen of $\mathbf{2H^+}$ (O_1). As with $\mathbf{2H^+ \cdot W\_TS\_5_{ptc\text{-}3}}$, the removal of the N−$H_1$ proton was more advanced than the change of other critical bond distances. Again, the N−H_1 distance had significantly increased (1.03 to 1.81 Å) and the O_2−H distances of the explicit water resembled H_3O^+. The progress of the Wiberg bond indices at $\mathbf{2H^+ \cdot W\_TS\_5_{ptc\text{-}5}}$ indicated that the transfer of proton H_2 from the solvent water to O_1 was only ∼20% completed compared to ∼80% completion for the transfer of the N−H proton to the explicit solvent water molecule.

A reaction coordinate diagram for the proton-transport catalyzed conversion of $\mathbf{2H^+}$ to **5** is shown in Figure 5, and the associated ΔG and $\Delta G^{\ddagger}$ are given in Table 5 for all of the substituents studied. The overall process of $\mathbf{2H^+}$ to **5** ($\Delta G_{\mathbf{2H^+ \rightarrow 5}}$) was always exergonic; however, the process was noticeably more exergonic for electron donating substituents. This assertion was supported by examining the Mulliken charges of the sulfur and carbon atoms for R = CH_3 and R = CF_3. The Mulliken charge on the sulfur increased from 0.4 for $\mathbf{2H^+}$ to 0.8 for **5** for both R groups. Thus, the effect of the electron-withdrawing trifluoromethyl group would be to destabilize **5**. Stabilization of the positive charge by the electron donating groups would be expected to increase as the positive charge shifts from the nitrogen to the sulfur. Thus, the increased stabilization of the partial positive charge was considered the most important contribution to the observed variance of the reaction energies for electron donating and electron withdrawing substituents.

Without implicit solvation, hydrogen bonding between $\mathbf{2H^+}$ and an explicit water molecule ($\mathbf{2H^+ \cdot W}$) was always energetically favorable ($\Delta G_{\mathbf{2H^+ \rightarrow 2H^+ \cdot W}}$). The barriers associated with $\mathbf{2H^+ \cdot W\_TS\_5_{ptc\text{-}3}}$ and $\mathbf{2H^+ \cdot W\_TS\_5_{ptc\text{-}5}}$ ($\Delta G^{\ddagger}_{\mathbf{2H^+ \cdot W\_TS\_5ptc\text{-}3}}$ and $\Delta G^{\ddagger}_{\mathbf{2H^+ \cdot W\_TS\_5ptc\text{-}5}}$) were comparable and ranged from 15 to 25 kcal/mol. Compared to the unassisted 1,2-hydrogen shift ($\Delta G^{\ddagger}_{\mathbf{2H^+\_TS\_5 \cdot W}}$), proton-transport catalysis by the explicit water molecule reduced the barrier to the proton transfer by approximately 10 kcal/mol.

Implicit solvation had little effect on the geometries of the critical structures. Implicit solvation stabilized $\mathbf{2H^+}$ to a greater degree than $\mathbf{2H^+ \cdot W}$ due to delocalization of the charge. Since $\mathbf{2H^+ \cdot W}$ was less stable than the completely separated reactants ($\mathbf{2H^+}$ + H_2O), it was of no relevance to the energetics of the reaction, and the reported PCM-MP2/6-311+G(3df,2p) value for $\Delta G^{\ddagger}_{\mathbf{2H^+ \cdot W\_TS\_5ptc\text{-}3}}$ and $\Delta G^{\ddagger}_{\mathbf{2H^+ \cdot W\_TS\_5ptc\text{-}5}}$ was the difference in free energy between $\mathbf{2H^+}$ and the corresponding transition state. Excluding R = CF_3, the values of $\Delta G^{\ddagger}_{\mathbf{2H^+ \cdot W\_TS\_5ptc\text{-}3}}$ and $\Delta G^{\ddagger}_{\mathbf{2H^+ \cdot W\_TS\_5ptc\text{-}5}}$ were between 20 and 25 kcal/mol at the PCM-MP2/6-311+G(3df,2p) level of theory. Implicit solvation had little effect on $\Delta G_{\mathbf{2H^+ \rightarrow 5}}$ and the aforementioned effect of electron-withdrawing groups was still observed.

A consistent feature for all the transition states, with and without implicit solvation, was that only slight protonation of the oxygen was required to start the N−O bond cleavage process. Therefore, the major component of the activation barrier was the removal of the N−H proton, which was evident by the advanced progress of the N−H_1 bond cleavage shown in Table 4.

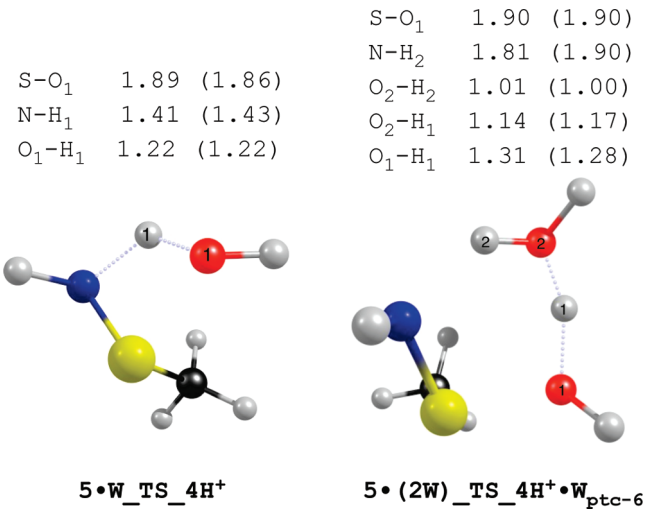

FIGURE 6. Graphical renderings of the B3LYP/6-31G(d) structures for the reaction pathway leading from **5** to $\mathbf{4H^+}$ displaying the B3LYP/6-31G(d) and (PCM-B3LYP/6-31G(d)) bond lengths (Å) for R = CH_3.

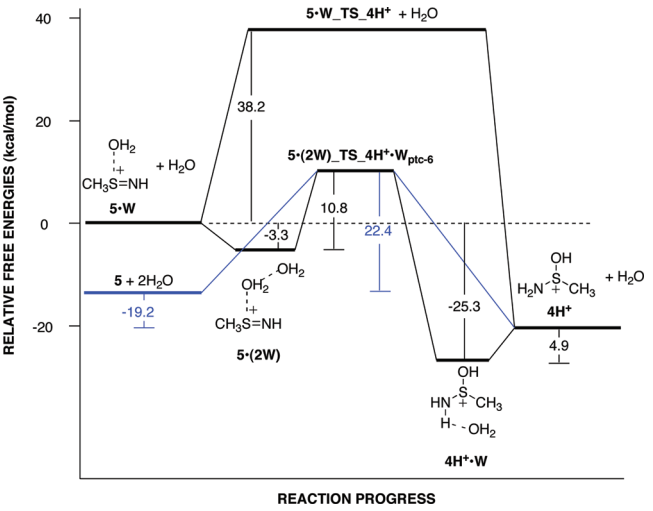

FIGURE 7. Reaction coordinate diagram for $\mathbf{5 \cdot W}$ to $\mathbf{4H^+}$ using CBS-QB3 (black line) free energies at 298.15 K. The blue line and free energy values represent the predicted PCM-MP2/6-311+G-(3df,2p)//PCM-B3LYP/6-31G(d) pathway.

Since the magnitude of $\Delta G^{\ddagger}$ was dependent upon the removal of the N−H hydrogen, the inclusion of the explicit water ($\mathbf{2H^+ \cdot W\_TS\_5_{ptc\text{-}3}}$ and $\mathbf{2H^+ \cdot W\_TS\_5_{ptc\text{-}5}}$) lowered $\Delta G^{\ddagger}$ by providing a base to assist with the removal of the N−H proton (H_1). Additionally, since the explicit water was in essence H_3O^+ in both $\mathbf{2H^+ \cdot W\_TS\_5_{ptc\text{-}3}}$ and $\mathbf{2H^+ \cdot W\_TS\_5_{ptc\text{-}5}}$, the protons ($H_1$ or H_2) being transferred to O_1 were essentially equivalent. Thus, the expected benefit of a 5-membered transition state over a 3-membered transition state was negated. Overall, the rate constant for the formation of **5** would be expected to be dependent upon the pK_a of $\mathbf{2H^+}$. This assertion was supported by the observance that for $\mathbf{2H^+}$ R = CF_3, where the reported pK_a value was 5.7, the values of $\Delta G^{\ddagger}$ were consistently 5 kcal/mol lower than the other R groups examined.

Intuitively, the reaction of **5** and water should be rapid, and thus, the expected rate-determining step for the conversion of **2** to sulfinamide (**4**) was the formation of **5**. To confirm this assertion, the transformation of **5** to the protonated form of **4** ($\mathbf{4H^+}$) was investigated. The pK_a of $\mathbf{4H^+}$ was found to be 15.0 at the PCM-MP2/6-311+G(3df,2p)//PCM-B3LYP/6-31G(d) level of theory, and thus, **4** would be expected to exist as $\mathbf{4H^+}$ in neutral aqueous solution. Nucleophilic attack of the sulfur atom of **5** by water and a subsequent proton transfer from the water moiety to nitrogen would yield $\mathbf{4H^+}$. This reaction was found to proceed through a four-membered transition state ($\mathbf{5 \cdot W\_TS\_4H^+}$), shown in Figure 6, where the proton transfer was synchronous with S−O bond formation. The reaction coordinate diagram for this path is shown in Figure 7. As would be expected for a four-membered transition state, the $\Delta G^{\ddagger}$ for this path was substantial (38.2 kcal/mol).

Inclusion of an explicit water was examined to determine the effect of proton-transport catalysis. As seen in Figure 7, a trimolecular complex ($\mathbf{5 \cdot (2W)}$) between **5** and two waters was slightly more stable than $\mathbf{5 \cdot W}$. A six-membered transition state ($\mathbf{5 \cdot (2W)\_TS\_4H^+ \cdot W_{ptc\text{-}6}}$) that led from $\mathbf{5 \cdot (2W)}$ to a bimolecular complex between $\mathbf{4H^+}$ and water ($\mathbf{4H^+ \cdot W}$) was found. Without the inclusion of implicit solvation, the overall ΔG of $\mathbf{5 \cdot W}$ to $\mathbf{4H^+}$ was over 20 kcal/mol exergonic with a $\Delta G^{\ddagger}$ of only 10.8 kcal/mol. Again, since the positive charge of **5** was delocalized in the transition state $\mathbf{5 \cdot (2W)\_TS\_4H^+ \cdot W_{ptc\text{-}6}}$, water would be expected to stabilize the transition state less than the reactant. Thus, the increase in $\Delta G^{\ddagger}$ (22.4 kcal/mol) with implicit solvation was expected.

As expected, examination of relative energies of the transition states revealed that the rate-determining step for the rearrangement of $\mathbf{2H^+}$ into $\mathbf{4H^+}$ was the first step. As seen in Figure 8, the unassisted 1,2-hydrogen shift $\mathbf{2H^+\_TS\_5 \cdot W}$ was 16.1 kcal/mol above $\mathbf{5 \cdot W\_TS\_4H^+}$ at the CBS-QB3 level of theory. Likewise, for the proton-transport-catalyzed conversion of $\mathbf{2H^+}$ to $\mathbf{4H^+}$, $\mathbf{2H^+ \cdot W\_TS\_5_{ptc\text{-}3}}$ was 27.0 kcal/mol above $\mathbf{5 \cdot (2W)\_TS\_4H^+ \cdot W}$ when implicit solvation was considered. Inspection of the relative free energies for the proton-transport catalyzed rearrangement in the gas phase (Figure S1, Supporting Information) also confirmed the first step as rate-determining.

IIIC. Reactions Leading from *N*-Hydroxysulfenamides (2) to Disulfides (3). A reaction between the putative intermediate **2** and an additional thiol moiety (Pathway B, in Scheme 1) was postulated to lead to the observed disulfide product. Nucleophilic substitution reactions at the sulfur atom have been investigated by a number of theoretical methods.[26,50−54] Depending upon the identity of the nucleophile, leaving group, and computational methods employed, substitution at the sulfur atom was suggested to proceed by either a S_N2 or an addition−elimination mechanism; however, a consistent feature of both mechanisms was backside attack by the nucleophile. The reaction between **2** and a thiolate yielding **3** and hydroxyamide base ($NHOH^-$) was considered; however, the thermodynamics of the reaction were unfavorable for all of the substituents. For example, the lowest value of ΔG for the

(50) Hayes, J.; Bachrach, S. *J. Phys. Chem. A* **2003**, *107* (39), 7952–7961.
(51) Bachrach, S.; Mulhearn, D. *J. Phys. Chem.* **1996**, *100* (9), 3535–3540.
(52) Bachrach, S.; Chamberlin, A. *J. Org. Chem.* **2003**, *68* (12), 4743–4747.
(53) Bachrach, S.; Woody, J.; Mulhearn, D. *J. Org. Chem.* **2002**, *67* (25), 8983–8990.
(54) Wu, X.-P.; Sun, X.-M.; Wei, X.-G.; Ren, Y.; Wong, N.-B.; Li, W.-K. *J. Chem. Theory Comput.* **2009**, *5* (6), 1597–1606.

TABLE 6. Activation and Reaction Energies for the Reaction Pathway Leading from $2H^+$ to $3H^+$[a]

R	level of theory	$\Delta G_{2H^+ \rightarrow 2H^+ \cdot 1}$	$\Delta G^{\ddagger}_{2H^+ \cdot 1\_TS\_3H^+ \cdot NH2OH}$	$\Delta G_{2H^+ \cdot 1 \rightarrow 3H^+ \cdot NH2OH}$	$\Delta G_{2H^+ \rightarrow 3H^+}$
H					
	CBS-QB3	−2.2	8.3	0.6	9.0
	PCM-MP2/6-311+G(3df,2p)[b]		26.0		18.0
CH_3					
	CBS-QB3	−3.5	2.7	−2.9	−2.8
	PCM-MP2/6-311+G(3df,2p)[b]		13.6		6.4
CF_3					
	CBS-QB3	2.2	11.5	10.4	15.8
	PCM-MP2/6-311+G(3df,2p)[b]		32.9		28.0
Ph					
	MP2/6-311+G(3df,2p)[c]	−5.7	2.4	3.5	−7.4
	PCM-MP2/6-311+G(3df,2p)[b]		15.1		7.6
Cys					
	MP2/6-311+G(3df,2p)[c]	0.5	8.4	6.8	−7.2
	PCM-MP2/6-311+G(3df,2p)[b]		--[d]		2.7

[a]All Gibbs free energies at 298.15 K. [b]Single points at PCM-B3LYP/6-31G(d) geometries. [c]CBS-QB3 failed, single points at B3LYP/6-31G(d) geometries. [d]Failed to optimize geometry.

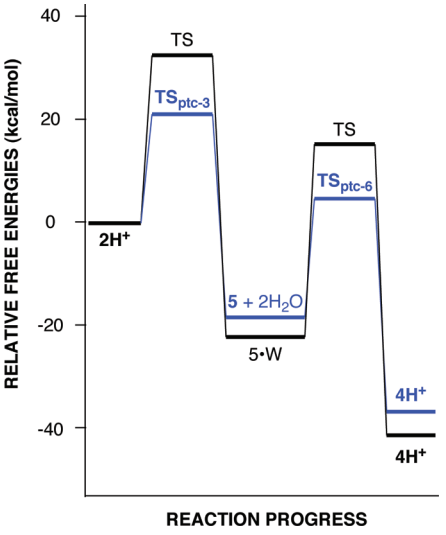

FIGURE 8. Reaction coordinate diagrams depicting free energies at 298.15 K for the rearrangement of $2H^+$ to $4H^+$. Black represents the unassisted path (CBS-QB3), and blue represents the proton-transport catalyzed path (PCM-MP2/6-311+G(3df,2p)//PCM-B3LYP/6-31G(d)).

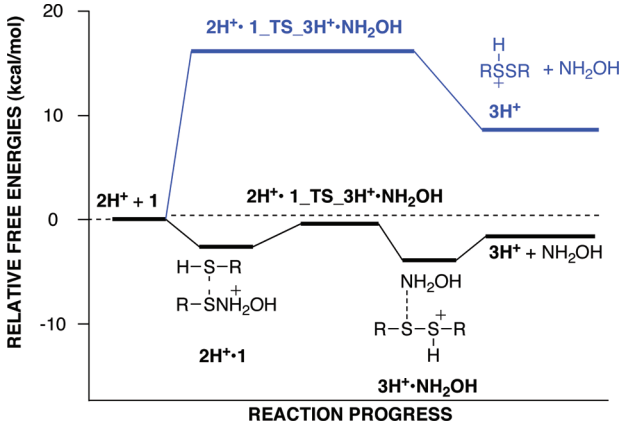

FIGURE 9. Reaction coordinate diagram for $2H^+$ + **1** to $3H^+$ at the CBS-QB3 (black line) and PCM-MP2/6-311+G(3df,2p)//PCM-B3LYP/6-31G(d) (blue line) levels of theory at 298.15 K for R = CH_3.

reaction was 25.2 kcal/mol ((PCM-MP2/6-311+G(3df,2p) for R = CH_3). Given the pK_a of $2H^+$ and that $NHOH^-$ was implausible as a leaving group, substitution by nucleophilic backside attack of $2H^+$ was used to examine the mechanism of disulfide formation.

As shown in Figure 9, the potential energy surface for the reaction of $2H^+$ with RSH (**1**) has the morphology of a S_N2 mechanism in the gas and condensed phases. The values for ΔG and $\Delta G^{\ddagger}$ for the various R groups are given in Table 6. In the gas phase, the transition state $2H^+ \cdot 1\_TS\_3H^+ \cdot NH_2OH$ was found to connect $2H^+ \cdot 1$, Figure 9, with an ion-dipole complex ($3H^+ \cdot NH_2OH$) between the conjugate acid of the disulfide ($3H^+$) and NH_2OH. Local minimum geometries for $2H^+ \cdot 1$ and $3H^+ \cdot NH_2OH$ were also found using PCM-B3LYP/6-31G(d); however, $2H^+ \cdot 1$ and $3H^+ \cdot NH_2OH$ were endergonic in relation to the completely separated reactants and products. Thus, $2H^+ \cdot 1\_TS\_3H^+ \cdot NH_2OH$ connected the solvent separated reactants ($2H^+$ and **1**) and the protonated form of the disulfide ($3H^+$) and NH_2OH. The pK_a of $3H^+$ (R = CH_3) was found to be −0.1 at the PCM-MP2/6-311+G(3df,2p)//PCM-B3LYP/6-31G(d) level of theory. Thus, in aqueous solution, the deprotonation of $3H^+$ would be expected to lead to the essentially irreversible formation of the disulfide (**3**).

Examination of the equilibrium geometries, as shown for R = CH_3 in Figure 10, revealed significant differences existed for ion−dipole complex ($2H^+ \cdot 1$) in the gas and condensed phase. When implicit solvation was included, the S−N bond of $2H^+ \cdot 1$ had only increased by 0.08 Å, compared to $2H^+$, and the S−S distance was still 2.96 Å. In both cases, the S−S bond length had nearly reached the equilibrium distance for the product ($3H^+$) at the transition state ($2H^+ \cdot 1\_TS\_3H^+ \cdot NH_2OH$), which was consistent with the endergonic nature of the reaction. Though the formation of $3H^+$ was endergonic in solution, the overall reaction would be driven forward by the deprotonation of $3H^+$ (R = CH_3, pK_a = −0.1). As would be expected for an S_N2 reaction between a neutral nucleophile and a charged electrophile, aqueous solvation increases the $\Delta G^{\ddagger}$ compared to the gas phase due to delocalization of the charge in the transition state. Unfortunately, for R = Cys, the location of a PCM-B3LYP/6-31G(d)-optimized transition state structure was prevented by convergence problems. An estimate of $\Delta G^{\ddagger}_{2H^+ \cdot 1\_TS\_3H^+ \cdot NH2OH}$ for R = Cys can be made by noting that the values of $\Delta G^{\ddagger}_{2H^+ \cdot 1\_TS\_3H^+ \cdot NH2OH}$ for the other substituents were approximately 5−10 kcal/mol greater than the corresponding $\Delta G_{2H^+ \rightarrow 3H^+}$. The value of $\Delta G_{2H^+ \rightarrow 3H^+}$ for R = Cys was 2.7 kcal/mol. Therefore, the value of $\Delta G^{\ddagger}_{2H^+ \cdot 1\_TS\_3H^+ \cdot NH2OH}$ for

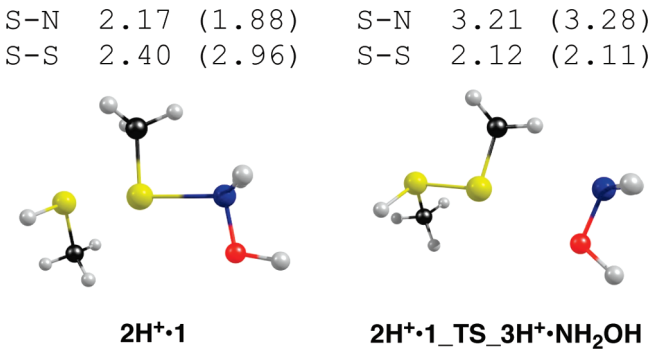

FIGURE 10. Graphical renderings of the B3LYP/6-31G(d) structures for the reaction between $\mathbf{2H}^+$ and **1** leading to $\mathbf{3H}^+$ displaying the B3LYP/6-31G(d) and (PCM-B3LYP/6-31G(d)) bond distances (Å) for R = CH_3.

R = Cys would be expected to be in the range of 8−13 kcal/mol. Thus, all of the results were consistent with an S_N2 mechanism for the reaction of **1** and $\mathbf{2H}^+$ in solution.

In the gas phase, $\mathbf{2H}^+\cdot\mathbf{1}$ had a significantly different structure than the local minimum found with implicit solvation. Noticeably, the S−S distance had been reduced to 2.40 Å compared to 2.96 Å in solution, and the S−N distance had lengthened nearly 0.4 Å. Analysis of the Wiberg bond indices found a value of 0.61 and 0.37 for the S−S and S−N bonds, respectively. Therefore, $\mathbf{2H}^+\cdot\mathbf{1}$ was more like a three-centered two-electron bonded intermediate than an intermolecular complex in the gas phase. Thus, it was considered that structure $\mathbf{2H}^+\cdot\mathbf{1}$ was the intermediate of an addition−elimination mechanism. However, a careful relaxed scan found that the potential energy surface gradually increased as the S−S bond distance was increased to 4.0 Å. Thus, at the B3LYP/6-31G(d) level of theory, there appeared to be no barrier or intermediates on the reaction pathway for the reaction of $\mathbf{2H}^+$ and **1** leading to $\mathbf{2H}^+\cdot\mathbf{1}$.

Though the overall trends were consistent, the identity of the R groups had a greater influence on the magnitude of the formation of the disulfide than on the reactions associated with pathway A. Consistent with the trends noted for pathway A, electron-withdrawing groups were more endergonic and had higher activation barriers. The influence of the R group on disulfide formation could be attributed to the increased positive charge on the sulfur in $\mathbf{3H}^+$ compared to $\mathbf{2H}^+$. Again, this assertion was supported by examining the Mulliken charges of the sulfur and carbon atoms for R = CH_3 and CF_3. The Mulliken charge on the sulfur increased by 0.08 for $\mathbf{3H}^+$ compared to $\mathbf{2H}^+$ for both R groups. The charge on the carbon was approximately 0.65 for R = CF_3 and only 0.10 for R = CH_3 for both $\mathbf{2H}^+$ and $\mathbf{3H}^+$. Therefore, the increase of 0.08 for R = CF_3 would be more energetically unfavorable due to the large positive charge on carbon. Similar arguments can be used to explain why $\Delta G_{\mathbf{2H}^+\rightarrow\mathbf{2H}^+\cdot\mathbf{1}}$ was only positive for R = CF_3. Therefore, greater destabilization of the charge in the product compared to the reactant was reflected in the magnitudes of ΔG and $\Delta G^{\ddagger}$ of the reaction.

IIID. Comparison of Pathway A to Pathway B. Since both HO^- and $NHOH^-$ are poor leaving groups, it can be intuitively concluded that neither pathway A nor pathway B are likely to occur without the protonation of **2**. The reaction pathways and calculated pK_a of ~13 for $\mathbf{2H}^+$ suggests that $\mathbf{2H}^+$ is the reactive form of **2** under physiological conditions. Once formed, the prevalence of a particular pathway would be expected to depend upon the pK_a of $\mathbf{2H}^+$, the solvation environment, and the availability of **1** or a general base.

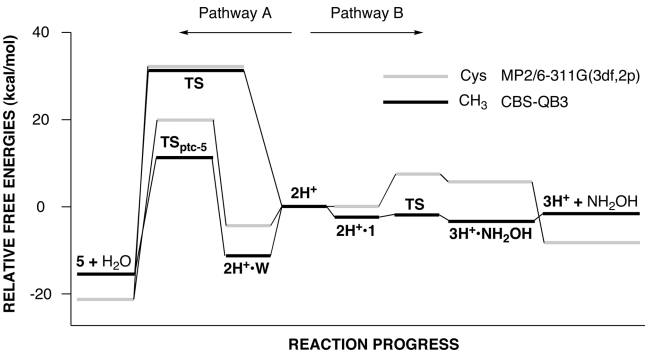

FIGURE 11. Reaction coordinate diagram comparing pathway A to pathway B for R = CH_3 and R = Cys.

TABLE 7. Comparison of the Activation and Reaction Energies for the First Steps Associated with Pathway A and Pathway B with Implicit Solvation[a]

R	$\Delta G^{\ddagger}_{\mathbf{2H}^+\cdot\mathbf{W\_TS\_5ptc\text{-}3}}$ (path A)[b]	$\Delta G^{\ddagger}_{\mathbf{2H}^+\cdot\mathbf{1\_TS\_3H}^+\cdot\mathbf{NH2OH}}$ (path B)[b]
H	22.2	26.0
CH_3	19.8	13.6
CF_3	11.8	34.7
Ph	24.9	15.1
Cys	23.0	~10[c]

[a]All Gibbs free energies in kcal/mol at 298.15 K. [b]PCM-MP2/6-311+G(3df,2p)//PCM-B3LYP/6-31G(d) values. [c]Estimated as 7 kcal/mol higher than $\Delta G_{\mathbf{2H}^+\rightarrow\mathbf{3H}^+}$.

Without the inclusion of implicit solvation, the results obtained are more similar to reactions that would occur in a hydrophobic environment than in an aqueous solution. In the absence of a proton-transport catalyst, the 1,2-hydrogen shift from the nitrogen to the oxygen of $\mathbf{2H}^+$ has a larger barrier ($\Delta G^{\ddagger}_{\mathbf{2H}^+\_\mathbf{TS\_5\cdot W}}$), as shown in Figure 11. Therefore, assuming the site was accessible to thiols, the prevailing pathway would be pathway B due to its lower activation barriers. However, the addition of explicit water reduced the rate-determining $\Delta G^{\ddagger}$ to the formation of **5** by approximately 10 kcal/mol by acting as proton−transport catalyst ($\mathbf{2H}^+\cdot\mathbf{W\_TS\_5}_{\mathbf{ptc\text{-}5}}$). Thus, the specific environment is expected have a substantial influence on the likelihood of the multistep rearrangement of $\mathbf{2H}^+$ into **4**. As a result, in a biological environment, pathway A is expected to compete with pathway B if RSH cannot reach $\mathbf{2H}^+$, the pK_a of $\mathbf{2H}^+$ is decreased, or a proton-transport catalyst assists the 1,2-hydrogen shift.

In aqueous solution, the prevailing pathway would be expected to be dependent upon the concentration of **1** and the pK_a of $\mathbf{2H}^+$. Pathway A is expected to be irreversible in water since $\Delta G_{\mathbf{2H}^+\rightarrow\mathbf{4H}^+}$ was calculated as −36.4 kcal/mol (R = CH_3), and pathway B should be irreversible due to the pK_a of $\mathbf{3H}^+$ (−0.1). Since both pathways are expected to be irreversible, the reaction should be kinetically controlled, and therefore, the product ratio should be dictated by the difference in $\Delta G^{\ddagger}_{\mathbf{2H}^+\cdot\mathbf{1\_TS\_3H}^+\cdot\mathbf{NH2OH}}$ and $\Delta G^{\ddagger}_{\mathbf{2H}^+\cdot\mathbf{W\_TS\_5ptc\text{-}3}}$. For easier comparisons, Table 7 lists the $\Delta G^{\ddagger}_{\mathbf{2H}^+\cdot\mathbf{1\_TS\_3H}^+\cdot\mathbf{NH2OH}}$ and $\Delta G^{\ddagger}_{\mathbf{2H}^+\cdot\mathbf{W\_TS\_5ptc\text{-}3}}$, for the five different R groups. As seen in Table 7, the dominant pathway in solution will depend upon the identity of the R group. Electron withdrawing groups were predicted to favor the formation of the sulfinamide. This was the result of the lower pK_a favoring

pathway A and the disfavoring of pathway B due to the destabilization of positive charge on the sulfur. Conversely, electron-donating groups favor pathway B, presumably due to the increased ability to stabilize the positive charge on the sulfur. Unfortunately, a firm prediction for cysteine cannot be made due to the inability to find an equilibrium geometry at the PCM-B3LYP/6-31G(d) level. Using other examples as a guide, the $\Delta G^{\ddagger}_{\mathbf{2H+\cdot 1\_TS\_3H+\cdot NH2OH}}$ for R = Cys would be expected to be 5−10 kcal/mol higher than $\Delta G_{\mathbf{2H+\rightarrow 3H+}}$. Thus, a reaction between cysteine and HNO in solution would be expected to follow pathway B, which is consistent with the experimental data.[25,55]

IV. Conclusions

The results presented in this study have provided mechanistic insights into the reaction pathways associated with the reaction between HNO and thiols. These insights support the experimental findings and clarify which factors may influence the outcome of these reactions in a variety of settings. The reaction between HNO and thiols was found to depend upon loss of the S−H proton, which was consistent with proteins whose local environment were expected to create anionic cysteine residues being sensitized to inhibition by HNO.[12,22] The large activation barriers without the assistance of an explicit solvent water suggested that deprotonation of the thiol would be required for S−N bond formation. The observation that **6** was not a minimum on the potential energy surface indicated that protonation of the oxygen of HNO may also be required prior to or during the rate-determining step.

The *N*-hydroxysulfenamide intermediate formed from the reaction of HNO and a thiol was expected to protonate under most conditions. In aqueous solutions, the computed pK_a of the protonated disulfide ($\mathbf{3H^+}$) and $\Delta G_{\mathbf{2H+\rightarrow 4H+}}$ strongly suggested the competition between the two considered pathways would be kinetically controlled. Additionally, the extremely exergonic values of $\Delta G_{\mathbf{2H+\rightarrow 4H+}}$ suggested that the sulfinamide will be quite stable, and since there are no known systems for the reduction of sulfinamides, the prediction that the formation of a sulfinamide causes irreversible inhibition of proteins with critical cysteine residues was strengthened. In a hydrophobic environment, the calculated activation barriers strongly indicated that formation of a disulfide would be favored. This was consistent with the ability of GSH to prevent the irreversible inhibition of proteins in vitro. The formation of the sulfinamide would be expected to become more favorable if a base was present in the local environment and with stronger electron-withdrawing substituents. In solution, greater competition between the two pathways was predicted. However, formation of the disulfide was still expected to be favored in most conditions. Electron-withdrawing substituents were predicted to favor the formation of the sulfinamide.

Acknowledgment. We thank Saint Louis University and the National Center for Supercomputing Applications for support of this research. We thank Mike Lewis for many helpful discussions.

Supporting Information Available: Coordinates of all optimized geometries, calculated vibrational frequencies, single-point energies, and all of the tables in expanded form. This material is available free of charge via the Internet at http://pubs.acs.org.

(55) Donzelli, S.; Espey, M. G.; Thomas, D. D.; Mancardi, D.; Tocchetti, C. G.; Ridnour, L. A.; Paolocci, N.; King, S. B.; Miranda, K. M.; Lazzarino, G.; Fukuto, J. M.; Wink, D. A. *Free Radic. Biol. Med.* **2006**, *40* (6), 1056–1066.